Resolving the effects of frequency-dependent damping and quantum phase diffusion in $YBa_2Cu_3O_{7-x}$ Josephson junctions

D. Stornaiuolo,[1,*] G. Rotoli,[2] D. Massarotti,[1,3] F. Carillo,[4] L. Longobardi,[1,2] F. Beltram,[4] and F. Tafuri[1,2]
[1]*CNR-SPIN Napoli, Complesso Universitario di Monte Sant'Angelo, 80126 Napoli, Italy*
[2]*Dipartimento di Ingegneria Industriale e dell'Informazione, Seconda Università di Napoli, Aversa (CE), Italy*
[3]*Dip. di Scienze Fisiche, Università degli Studi di Napoli Federico II, Napoli, Italy*
[4]*NEST, Scuola Normale Superiore, I-56126 Pisa, Italy*

(Received 17 September 2012; revised manuscript received 30 January 2013; published 25 April 2013)

We report on the study of the phase dynamics of high-critical-temperature superconductor Josephson junctions. We realized $YBa_2Cu_3O_{7-x}$ grain boundary biepitaxial junctions in the submicron scale using low-loss substrates and analyzed their dissipation by comparing the transport measurements with Monte Carlo simulations. The behavior of the junctions can be fitted using a model based on two quality factors, which results in a frequency-dependent damping. Moreover, our devices can be designed to have Josephson energy of the order of the Coulomb energy. In this unusual energy range, phase delocalization strongly influences the device's dynamics, promoting the transition to a quantum phase diffusion regime. We study the signatures of such a transition by combining the outcomes of Monte Carlo simulations with the analysis of the device's parameters, the critical current, and the temperature behavior of the low-voltage resistance R_0.

DOI: 10.1103/PhysRevB.87.134517 PACS number(s): 74.50.+r, 85.25.Cp

I. INTRODUCTION

A correct understanding of the phase dynamics of a Josephson circuit relies on the possibility of distinguishing the contributions to dissipation coming from the junction itself from those due to the external circuit. This is especially relevant in the moderately damped regime for junctions with low critical current. High-temperature superconductor (HTS) Josephson junctions (JJs) often fall in this category. Their phase dynamics is made particularly rich by the HTS unconventional superconductivity.[1–3] The high values of the critical temperature ($T_c \approx 90$ K) and of the superconducting gap ($\Delta \approx 20$ meV) impose a unique energy scale on HTS JJs. Some effects generally observed in HTS junctions, for example, the fact that the values of the $I_c R_n$ parameter (with I_c and R_N being the critical current and normal state resistance, respectively) are, on average, one order of magnitude lower than the expected value of 2Δ, may signify the relevance of other energy scales in these devices.[3–5] One possibility is the Thouless energy associated with single nanoscale channels in a filamentary approach to transport across the grain boundary (GB).[6]

Despite this complexity, recent experiments demonstrate that macroscopic quantum phenomena can be observed also in HTS JJs,[7–9] revealing coherence beyond expectations. Ultrasmall HTS junctions were also used to realize single electron transistors with unprecedented energy resolution[10] and were proposed for the fabrication of ultrasensitive superconducting quantum interference devices to use in the detection of small spin systems.[11,12] These studies confirm the interest in nanoscale HTS devices and the need for a systematic and reliable study of their phase dynamics.

A detailed analysis of phase dynamics in moderately damped low-temperature superconductor (LTS) JJs was performed by Kautz and Martinis in the early 1990s.[13] Here the need for a frequency-dependent damping to fully account for the phenomenology of the junctions emerges, with clear indications of distinct behaviors at low and high frequencies. These arguments offer the possibility to disentangle the quality factor of the junction from that of the external circuit. More recently, moderately damped JJs based on both LTS and HTS and operating in the phase diffusion regime were investigated through the analysis of the switching current distribution (SCD) histograms.[14–16] All these devices are, however, characterized by values of the Josephson energy $E_J = \hbar I_0/2e$ (where I_0 is the critical current in the absence of thermal fluctuations) much larger than those of the charging energy $E_c = e^2/2C$ (where C is the junction capacitance). Devices characterized by $E_J \approx E_c$, on the other hand, were studied by Iansiti *et al.*[17] using Sn-based junctions with a nominal area of $\sim 0.1\ \mu m^2$ and I_c in the range 1–10 nA. It was shown that this energy scale favors access to a quantum phase diffusion regime, which is quite unexplored and whose nature is still unsettled.[15–18]

In this work we study the phase dynamics of submicron HTS JJs in the moderately damped regime using the tools developed for LTS JJs. We have realized $YBa_2Cu_3O_{7-x}$ (YBCO) junctions with lateral size down to 600 nm on $(La_{0.3}Sr_{0.7})(Al_{0.65}Ta_{0.35})O_3$ (LSAT) substrates. The reduction of the junctions' size allows one to minimize the influence of the GB microstructure on the transport properties of the devices,[12,19,20] while the use of the LSAT substrate reduces the parasitic capacitance present in the more common $SrTiO_3$ (STO)-based junctions.[21] Using Monte Carlo simulations, we extract the frequency-dependent damping of these devices and show that, for a particular range of parameters, the quantum phase diffusion regime can be attained.

II. EXPERIMENT

The junctions studied in the present work were realized following the design reported in Refs. 20,22, and 23. A CeO_2 thin film is deposited using rf magnetron sputtering on a (110)-oriented LSAT substrate and patterned using photolithography and ion-beam etching (IBE). A 200-nm YBCO film is then

 ©2013 American Physical Society

deposited using inverted cylindrical magnetron sputtering, obtaining (001) growth on the CeO_2 seed layer and (103) growth on the LSAT substrate, and it is subsequently covered with a protective gold layer (100 nm thick). The definition of the submicron bridges is carried out using an electron beam lithography technique adapted to HTS requirements.[24] The electron beam pattern is transferred to a 80-nm-thick Ti layer which serves as a hard mask. The YBCO not covered by the Ti mask is removed using IBE, keeping the sample at low temperature ($-140\,^\circ$C) in order to minimize oxygen loss. After this, the Ti mask is removed by chemical etching in a highly diluted (1:20) HF solution. Finally, the protective gold layer is removed using the last step of low-energy IBE. In Figs. 1(a) and 1(c) scanning electron microscope images of 600-nm-wide devices (before the gold removal) are shown. The high quality of the YBCO film can be inferred from the systematic presence of elongated grains with a typical size of 1 μm in the (103) part and by the absence of impurities and outgrowths in the (001) part.[25]

The devices were measured down to 0.25 K using a four-contact technique. The measurement environment was magnetically shielded, and the lines were filtered using RC filters and two stages of copper powder filters.[26] Current vs voltage (I-V) characteristics of two typical devices, 1W and 6W, are shown in Figs. 1(b) and 1(d), respectively. The I-V characteristics are modulated by the magnetic field H [Figs. 1(e) and 1(f)], leading to a Fraunhofer-like $I_c(H)$ pattern for junction 1W.[3,27] Taking into account focusing effects,[28] the $I_c(H)$ pattern periodicity in the field points to an effective width of $\approx$500 nm for device 1W [Fig. 1(e)] and of $\approx$600 nm for device 6W [Fig. 1(f)]. These values are very close to the nominal dimensions of the devices. The critical current density J_c is 65 A/cm^2 for device 1W and 5 A/cm^2 for device 6W. The low J_c values of these devices are a consequence of oxygen depletion, occurring especially in the GB region.[29] This is a quite general feature of HTS JJs[3] and is expected to be of particular relevance when decreasing the size of the junction, as in this case. We have found that the devices realized using LSAT as a substrate are characterized by higher values of the normal-state resistance and are more affected by aging when compared with the ones fabricated on STO substrates. These microstructural factors could in this case mask the influence of the d-wave order parameter in determining the magnitude of J_c as a function of the junction misorientation.[22] Grains elongated in the current direction in device 1W [Fig. 1(a)], for instance, might be less exposed to oxygen desorption compared to grains leaning against the walls of the channel in device 6W [Fig. 1(c)], explaining the different values of I_c measured for these two devices.

The reduced values of J_c, on the other hand, offer the possibility of having access to JJ dynamical regimes which have been poorly explored. The Josephson energy E_J is $\approx$270 μeV (corresponding to 3 K) for device 1W and 70 μeV (corresponding to 0.8 K) for device 6W. These energies were calculated using the I_0 values obtained through comparison to numerical results, as described in Sec. IV. They are one or two orders of magnitude smaller than those measured for junctions where macroscopic quantum behavior has been demonstrated[8] and five orders of magnitude smaller than those observed in most HTS Josephson devices.[3,5] More importantly, for device

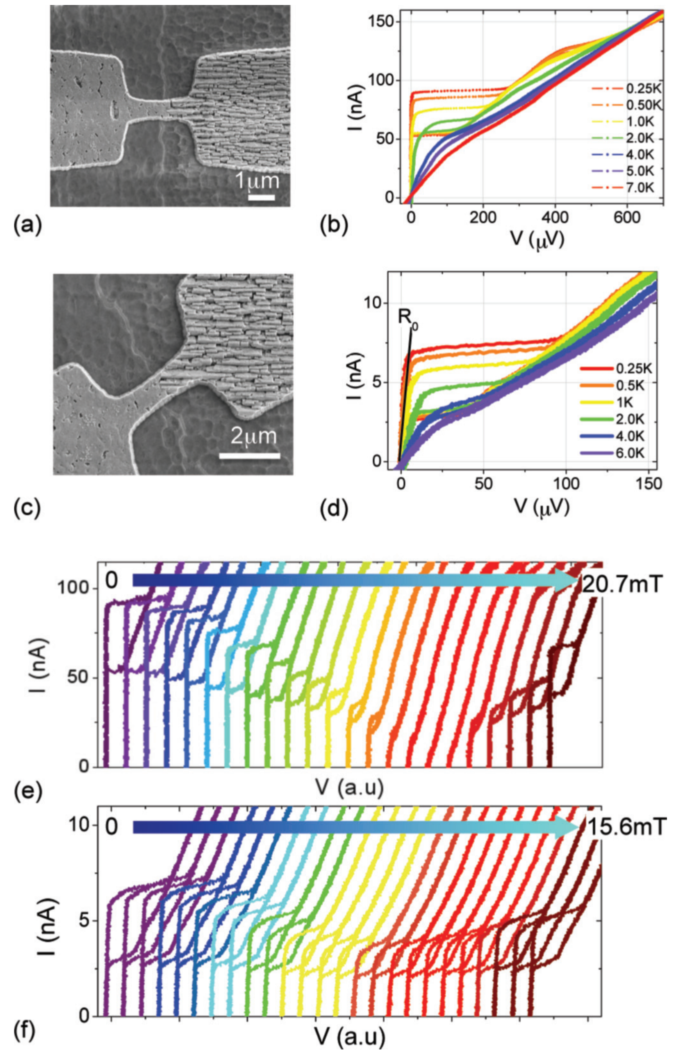

FIG. 1. (Color online) SEM images of devices (a) 1W and (c) 6W and (b) and (d) plots of the respective relative I-V characteristics measured at various temperatures. The width is 600 nm for both devices. (e) and (f) I-V measured at $T = 0.25$ K as a function of H (applied in the junction's barrier plane) for devices 1W and 6W, respectively. The curves were shifted horizontally for clarity. H is ramped from 0 to 20.7 mT in steps of 0.9 mT in (e) and from 0 to 15.6 mT in steps of 0.6 mT in (f).

6W, E_J is comparable to the charging energy E_c, as will be described in Sec. IV, placing this device in an uncommon and interesting energy range.

The I-V curves shown in Fig. 1 are highly hysteretic, with a difference between the critical (I_c) and the retrapping (I_r) current up to 70% at the lowest temperature [Fig. 1(d)]. The presence and the nature of hysteresis in the I-V curves of HTS junctions have been a matter of debate.[3] It is indeed difficult in these devices to disentangle the intrinsic capacitive effects in the GB barrier from extrinsic ones, deriving from the external circuit, also due to the high dielectric constant (above 10 000 at low temperatures[30]) of the STO substrates on which the junctions are commonly fabricated.[3,5,8,31] In the present work, we have used LSAT as a substrate, with a temperature-independent dielectric constant ϵ_r of 23.[32] As a consequence, the influence of the external circuit is greatly reduced.[20]

Remarkably, this neat hysteresis coexists with a slope at low voltage. The low-voltage slope is a hallmark of phase diffusion effects[13] and is visible in Fig. 1(b) (device 1W) for temperatures greater than 2K and in Fig. 1(d) (device 6W) in the whole temperature range, down to 0.25 K. The two phenomena, hysteresis and phase diffusion, can separately be understood in the framework of the washboard potential model for Josephson junctions.[27] On the other hand, their coexistence in the same I-V curve is unusual[13,17,33] and requires a finer analysis of the devices' properties and dynamics, which we will address in the following section.

III. THE TILTED WASHBOARD POTENTIAL MODEL FOR STUDYING JJ PHASE DYNAMICS

The behavior of a Josephson junction can be described, in the most general approach, by a Hamiltonian $\mathcal{H}$, which is a function of the phase difference φ between the superconductive electrodes:

$$\mathcal{H} = -4E_c\frac{\partial^2}{\partial\varphi^2} - E_J\cos\varphi, \tag{1}$$

where E_c and E_J are the aforementioned charging and Josephson energies, respectively.[18] E_c is commonly much smaller than E_J, both in the HTS and in the LTS cases; therefore the E_c term in Eq. (1) is usually disregarded. In this condition, the dynamics of the junction phase can be modeled as the motion of a fictitious particle of mass $m = C(\Phi_0/2\pi)^2$ in the "washboard" potential $U(\varphi) = -E_J[\cos\varphi + (I/I_0)\varphi]$, sketched in Fig. 2. This dynamics is well understood, both in the classical and in the quantum regimes.[27,34] For $I < I_0$ the potential U has local minima where the phase particle is trapped and oscillates at the plasma frequency $\omega_0 = \sqrt{2\pi I_0/C\Phi_0}$. An increase of I has the effect of tilting the potential and decreasing the barrier between two neighboring minima. Eventually, for $I = I_0$ the phase will escape from the well, and a voltage will appear at the junction's edges. Decreasing the bias current, the potential tilt will be reduced, and for $I = I_r$ the particle will be retrapped in a well, returning to the zero-voltage state.

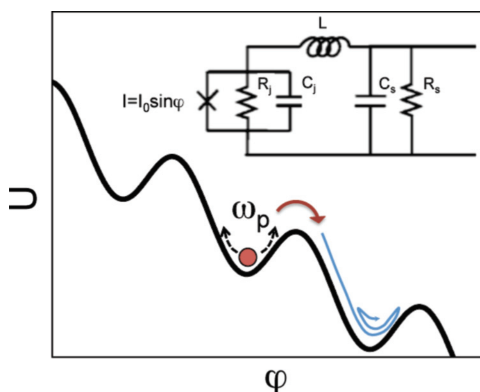

FIG. 2. (Color online) Tilted washboard potential of a Josephson junction. The red arrow indicates the effect of thermal activation, and the blue one indicates the recapturing of the fictitious phase particle in overdamped junctions. In the inset, the circuit considered in the frequency-dependent damping model is shown.

In the case of underdamped junctions, with quality factor $Q_0 = \omega_0 RC > 1$, we find $I_r < I_0$; therefore a hysteresis is present in the I-V characteristic. In the case of overdamped junctions ($Q_0 < 1$), only one stationary state, the one at rest at a potential minimum with zero voltage across the junction, is stable for $I < I_0$, and the I-V characteristics show no hysteresis.[27]

This picture is strictly valid only at zero temperature. At finite temperature, thermal noise activates the phase over the energy barrier, favoring a slip from the potential well for $I = I_c < I_0$ (red arrow in Fig. 2). In underdamped junctions, a single phase slip event is enough for the junction to switch to the running state. In overdamped junctions, on the other hand, after thermal slippage, the phase can be recaptured in the next well (blue arrow in Fig. 2). This prevents access to the running state and leads to the appearance of a nonzero voltage, manifesting as a "rounding" in the I-V curve at low currents. This regime is called phase diffusion.[18,27]

A. Frequency-dependent damping model

A more complete description of the Josephson phase dynamics can be achieved by incorporating the effects of the circuit the junction is embedded in. The effects of the external environment are taken into account through an additional quality factor Q_1.[13,35] In the case of HTS-based junctions, this external circuit is intrinsic and partly hidden because it is embedded in the GB and, in the case of off-axis biepitaxial junctions, in the (103)-oriented electrode.[8,31] The study of its contributions, as encoded in the damping of HTS devices, therefore becomes more challenging.

The effects of the embedding circuit become particularly interesting when $Q_1 < Q_0$. At the plasma frequency ω_0 (typically in the gigahertz range), the smaller quality factor Q_1 dominates the behavior of the whole system. The voltage state involving steady motion of the phase is instead dominated by the higher quality factor Q_0. Therefore, the system will exhibit a frequency-dependent damping, which explains the coexistence of hysteresis and phase diffusion,[13] as seen in our devices [Figs. 1(b) and 1(d)].

When E_c is comparable to E_J, the E_c term in Eq. (1) cannot be disregarded. Its presence leads to phase delocalization effects. The value of the ratio $x = E_c/E_J$ is a measure of how strongly the charging energy acts in delocalizing the phase, and is related to the width $\delta\varphi$ of the phase wave function $\psi(\varphi)$: $\delta\varphi = (x)^{1/4}$. For $x \ll 1$, $\psi(\varphi)$ is a narrowly peaked function, and the phase is localized and can be treated as a semiclassical quantity. For values of x greater than 1/4, on the other hand, the phase variable is sufficiently delocalized that quantum fluctuations cannot be neglected and quantum uncertainty, especially at low temperatures, has to be taken into account.[17] Phase delocalization leads to an increase in the probability for the phase to escape from the potential well, both in the thermal and in the quantum regimes. Multiple escapes and retrappings result in a finite resistance R_0 at low voltage; in the quantum regime, the value of R_0 saturates due to freezing out of the thermal fluctuations.

B. Numerical model

In order to model frequency-dependent damping in our devices, we use a two-Q model, following the work of Kautz and Martinis[13] (K-M model). The circuit considered is shown in the inset of Fig. 2.[36] Conservation of the current at nodes and the Josephson equations imply the following normalized Langevin equations for the phase φ and the voltage V_b at the external circuit capacitance C_s:

$$\ddot{\varphi} = Q_0^{-2}[(V_b - \dot{\varphi})(Q_0/Q_1 - 1) - \dot{\varphi} - \sin\varphi + \gamma_b + \gamma_{n1} + \gamma_{n2}], \tag{2}$$

$$\dot{V}_b = \rho Q_0^{-2}[(\dot{\varphi} - V_b) + \gamma_{n2}/(Q_0/Q_1 - 1)]. \tag{3}$$

In the equations above, time is normalized to $\hbar/2eI_0R_j = \omega_0^{-1}/Q_0$, and currents are normalized to the critical current I_0; $Q_0 = R_j\sqrt{2eI_0C_j/\hbar} = \omega_0R_jC_j$ and $Q_1 = (1/R_j + 1/R_s)^{-1}\sqrt{2eI_0C_j/\hbar} = \omega_0R_sC_j$. The term $(V_b - \dot{\varphi})(Q_0/Q_1 - 1)$ represents the normalized current through external load R_s, $\rho = R_jC_j/R_sC_s$ is the time constant ratio, γ_b is the normalized bias current, and γ_{n1}, γ_{n2} are the noise currents associated with the intrinsic resistor R_j and the external resistor R_s, respectively. These are modeled as Gaussian stochastic processes with zero mean and variance given by

$$\langle\gamma_{nk}(t),\gamma_{nk}(t')\rangle \equiv \sigma_k^2\delta(t-t') = \alpha_k\frac{2k_BT}{E_j}\delta(t-t'), \tag{4}$$

with $\alpha_1 = 1$ and $\alpha_2 = Q_0/Q_1 - 1$. This simple model is able to reproduce the main features of the experimental results[13] without the use of other parameters. Simulations of the Langevin equations have been made by generating Gaussian noise with the CERNLIB RANLUX routine.[37] Other details of the numerical integration can be found in Ref. 31. In order to capture the phase diffusion regime in I-V characteristics an average procedure was performed over 2000 or 3000 single I-V curves, depending on temperature. Each single I-V curve was generated by averaging over 2000 time units. Typical runs for simulations of Eqs. (2) and (3) will last from 2×10^6 to 4×10^6 normalized time units, i.e., 10^5 to 2×10^5 plasma periods.

In the next section, we will compare our experimental data with the frequency-dependent damping model. The low-temperature measurements of device 6W are then discussed in the framework of the quantum phase diffusion regime.

IV. COMPARISON BETWEEN NUMERICAL AND EXPERIMENTAL RESULTS

Figure 3(a) shows the comparison between the experimental data of device 1W measured at different temperatures (left panel) and numerical curves calculated using the two-Q model (right panel). Significant changes in the shape of the experimental I-V curves take place when cooling down from 2.0 K, where the I-V characteristics exhibit a small hysteresis of 15% and a pronounced rounding of the low-voltage branch, to 0.25 K, where the hysteresis reaches 40% and a sharp switch from the superconducting to the resistive branch is observed. The simulations in the right-hand side of Fig. 3 reproduce this behavior well: the evolution of the critical current, the amplitude of the hysteresis, and the coexistence of hysteresis and phase diffusion "rounding." The parameters used for the simulations are $Q_1 = 0.6 \pm 0.1$, $Q_0 = 5 \pm 0.5$, $I_0 = 130$ nA. These are consistent with a capacitance per unit area of 1.5×10^{-6} F cm^{-2} (as observed in wider junctions[20]), $\rho = 0.1$, and an effective resistance of 500 Ω. The experimental I_c measured at 0.25 K is only 70% of the I_0 value used for the simulations. This difference arises since the small E_J means that, at 0.25 K, $k_BT/E_J \sim 1/10$, so thermal noise currents (whose amplitude is proportional to $\sqrt{k_BT/E_J} \sim 0.31$) have a significant effect.

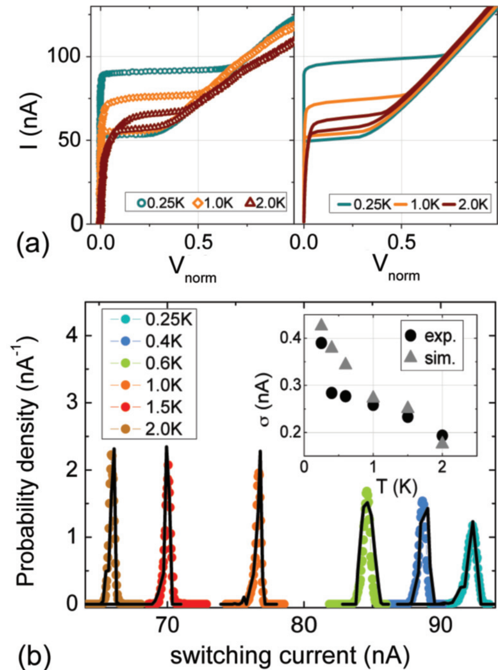

FIG. 3. (Color online) Transport properties of device 1W. (a) The experimental I-V characteristics (left panel, points) measured at $T = 0.25$, 1.0, and 2.0 K are compared with Monte Carlo simulations (right panel, solid lines) realized using the following parameters: $Q_1 = 0.6$, $Q_0 = 5$, and $I_0 = 130$ nA. (b) The comparison between experimental (points) and simulated (black solid lines) SCD histograms. The experimental SCD histograms were measured using a voltage criterion of 100 μV. The inset shows the behavior of the simulated (triangles) and experimental (dots) histogram width vs the temperature.

For this device, we have measured the SCD histograms at various temperatures, reported in Fig. 3(b). The standard deviation σ of the experimental SCD histograms decreases as the temperature increases [dots in the inset of Fig. 3(b)], as expected in the phase diffusion regime. The ratio between σ and the mean switching current is close to 10^{-3}, in agreement with that found in the literature.[38] In Fig. 3(b) we also show the fits to the SCD histograms (solid lines). These were realized using the following parameters: $Q_1 = 0.56$, $Q_0 = 2$, $I_0 = 130$ nA. The switching behavior of a JJ is a high-frequency phenomenon. Indeed, the study of the switching behavior of JJs in the moderately damped regime[14,16] is usually performed using a single-Q model to fit the experimental SCD histograms. Such a procedure works well when the condition $E_J \gg k_BT$ is satisfied and the quality factor is larger than 1.

In our case, $Q_1 = 0.56$; therefore, in order to preserve the underdamped dynamics of the phase after the escape process, a second quality factor Q_0 with a slightly increased value with respect to Q_1 had to be included in the model.

We point out that experimental reports showing the occurrence of phase diffusion effects both in the I-V curves and in the SCD histograms are extremely rare. This combined analysis has previously been carried out, to our knowledge, only in Ref. 38, where, contrary to what happens in our work, the main contribution to the damping of the devices comes from the external impedance, and the junction intrinsic resistance plays no significant role. In our case, the reduced value of E_J makes phase diffusion effects become evident not only in the behavior of the SCD histograms but also in the shape of the I-V characteristics, thereby offering two independent routes for the study of phase diffusion. An estimation of the high-frequency dissipation Q_1 for our device, for instance, is both an output of the K-M model and a necessity for numerically reproducing the experimental SCD histograms. Finally, we point out that, in previous experiments on off-axis biepitaxial junctions realized on LSAT substrates, the Q factor obtained via the simulation of SCD histograms was 1.3 ± 0.05.[16] This value is consistent with $Q_1 = 0.6 \pm 0.1$ found in the present work, taking into account that here I_c is one order of magnitude smaller and that high-frequency dissipation is larger for devices with reduced I_c.[39]

The analysis of the behavior of junction 1W reveals that the phase dynamics of YBCO submicron JJs characterized by low values of E_J is compatible with that expected, in the K-M approach, in the phase diffusion regime. A further reduction of E_J, making it comparable to E_c, induces a different behavior, as we will demonstrate for device 6W.

In Fig. 4 we compare the experimental I-V curves of device 6W (left panel) with simulations (right panel). In this case, it was impossible to find a single set of parameters which could reasonably reproduce the I-V curves in the complete range of temperatures. Agreement with the main features of the experimental data is obtained at high temperature ($T = 1.45$ K) by using the following parameters: $Q_1 = 0.6 \pm 0.1$, $Q_0 = 12 \pm 0.5$, and $I_0 = 35$ nA.[40] Remarkable deviations appear

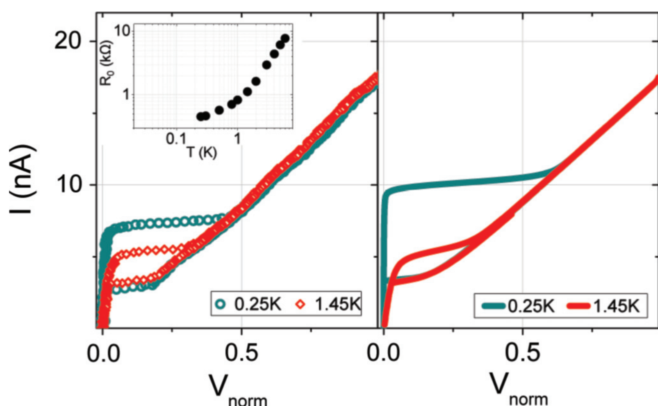

FIG. 4. (Color online) I-V characteristics of device 6W (points, left panel) measured at $T = 0.25$ and 1.45 K compared with Monte Carlo simulations (solid lines, right panel) made using $Q_1 = 0.6$, $Q_0 = 12$, and $I_0 = 35$ nA. In the inset the temperature dependence of the measured low-voltage resistance R_0 is shown.

TABLE I. Parameters of devices 1W and 6W. All the parameters refer to $T = 0.25$ K, except for Q_0, Q_1, and I_0 of device 6W, which refer to $T = 1.45$ K.

Device	E_J (μeV)	E_c (μeV)	x	Q_0	Q_1	I_0 (nA)
1W	270	45	0.16	5 ± 0.5	0.6 ± 0.1	130
6W	70	47	0.65	12 ± 0.5	0.6 ± 0.1	35

as the temperature is reduced to 0.25 K. We attribute such deviations to a transition from a classical regime, in which thermal fluctuations dominate, to a quantum regime, in which phase delocalization plays a key role in the dynamics. Indeed, for this device $x = E_c/E_J$ is 0.65 ($E_c \approx 47$ μeV; see Table I), leading to a region where phase delocalization effects are expected to be relevant and promoting quantum phase diffusion.[17,41]

The reduced value of I_c of device 6W (a factor of 10 lower compared to device 1W) is consistent with this estimation of the fundamental energies. As discussed in the previous section, x is related to the width of the phase function $\delta\varphi$ and therefore to the delocalization of the phase. For $x \approx 0.65$, $\delta\varphi$ is ≈ 0.9. Although phase φ is still confined in one well of the washboard potential, the barrier height of such a well, which depends on both E_J and E_c, is reduced, influencing the critical current. For $x > 1/4$, the critical current I_c is indeed scaled by E_B/E_J, where E_B is the binding energy:[17]

$$E_B \approx E_J 2x[(1 + 1/8x^2)^{1/2} - 1], \tag{5}$$

leading to a temperature-independent $I_c = 2eE_B/\hbar$, which is less than the value $I_0 = 2eE_J/\hbar$ which would be observed in the absence of quantum fluctuations. Using the values of E_J and x to calculate E_B, we obtain $I_c = 6.5$ nA, in good agreement with the experimental value measured at 0.25 K (see Fig. 4).

As mentioned in Sec. III, the temperature dependence of the finite resistance at low voltages R_0 is another indicator of the quantum phase diffusion state. Device 6W clearly shows such resistance, also at 0.25 K, as marked by the black line in Fig. 1(d). Iansiti *et al.*[17] report that the value and the behavior of R_0 depend on the ratio x. The R_0 values shown in the inset of Fig. 4 are consistent with those found in Ref. 17 resulting from numerical simulations using $x = 0.65$. Moreover, R_0 is proportional to the tunneling rate[17] $R_0 \approx \frac{h}{2eI}\Gamma$, and Γ can be calculated by using the Caldeira-Leggett approximation in the presence of dissipation.[42] Using this formula with an upper bound value of $R_0 \approx 500$ Ω, a damping Q of about 1 is obtained. This value is consistent with the high-frequency Q_1 factor inferred for this device (at high temperatures) using I-V simulations. More importantly, the R_0 of device 6W decreases with decreasing temperature and levels off around 0.3 K, as shown in the inset of Fig. 4. The saturation of R_0 marks the entrance into the quantum regime.[43]

From the estimated value of the plasma frequency $\omega_0 \approx 40$ GHz, we calculate a crossover temperature $T_{cr} = \hbar\omega_0/2\pi k_B$ between the classical and the quantum regimes of 120 mK.[44] Such an equation for the crossover temperature has been estimated in the regime $E_J \gg E_c$. In our case, since $E_J \approx E_c$, the binding energy is modified, the phase delocalization is

larger, and therefore the probability for quantum tunneling of the phase is increased. As a result, the crossover temperature between thermal and quantum activations is pushed up. Indeed our experimental data show that quantum tunneling of the phase influences the phase dynamics already at 0.3 K. We point out that junction 1W has similar values of ω_0 and T_{cr} (75 GHz and 155 mK, respectively), but the condition $E_c \ll E_J$ (see the values listed in Table I) results in negligible delocalization effects, and the dynamics of the junction is classical down to 0.25 K, as shown by the good agreement between the experimental data and the simulations (Fig. 3).

V. CONCLUSIONS

We have engineered YBCO grain boundary biepitaxial junctions in the submicron scale, down to 600 nm, and with reduced Josephson energy E_J. This regime is quite rare to achieve for HTS JJs and has been, up to now, little explored. The junction behavior can be simulated using a frequency-dependent damping model. The quality factors obtained by the fits indicate a moderately damped regime.[7,20,21] Classical phase diffusion, in a frequency-dependent approach, describes quite well the behavior of the devices, as far as $E_c \ll E_J$. When $E_J \approx E_c$, delocalization starts to play an important role in the phase dynamics, the temperature at which quantum effects start to influence the phase dynamics is increased, and a possible transition to a quantum phase diffusion regime occurs at $T \approx 0.3$ K.

This work is of relevance both for defining phase dynamics in HTS JJs in extreme limits and for the experimental search for quantum phase diffusion. More systematic studies will be required to obtain additional hints to the effects of microscopic factors, in particular the relation between a d-wave order parameter symmetry and dissipation.

ACKNOWLEDGMENTS

We acknowledge the support of MIUR-Italy through PRIN project "2009 Nanowire high critical temperature superconductor field-effect devices" and COST project, action MP-1201, "Nanoscale Superconductivity: Novel Functionalities through Optimized Confinement of Condensate and Fields."

*Present address: Department of Condensed Matter Physics, University of Geneva 24 Quai E.-Ansermet, CH-1211 Geneva 4, Switzerland; daniela.stornaiuolo@unige.ch

[1] C. C. Tsuei and J. R. Kirtley, Rev. Mod. Phys. **72**, 969 (2000).
[2] D. J. Van Harlingen, Rev. Mod. Phys. **67**, 515 (1995).
[3] F. Tafuri and J. R. Kirtley, Rep. Prog. Phys. **68**, 2573 (2005).
[4] R. Gross, L. Alff, A. Beck, O. M. Froehlich, D. Koelle, and A. Marx, IEEE Trans. Appl. Supercond. **7**, 2929 (1997).
[5] H. Hilgenkamp and J. Mannhart, Rev. Mod. Phys. **74**, 485 (2002).
[6] P. Lucignano, D. Stornaiuolo, F. Tafuri, B. L. Altshuler, and A. Tagliacozzo, Phys. Rev. Lett. **105**, 147001 (2010).
[7] T. Bauch, F. Lombardi, F. Tafuri, A. Barone, G. Rotoli, P. Delsing, and T. Claeson, Phys. Rev. Lett. **94**, 087003 (2005).
[8] T. Bauch, T. Lindstrom, F. Tafuri, G. Rotoli, P. Delsing, T. Claeson, and F. Lombardi, Science **311**, 56 (2006).
[9] K. Inomata, S. Sato, K. Nakajima, A. Tanaka, Y. Takano, H. B. Wang, M. Nagao, H. Hatano, and S. Kawabata, Phys. Rev. Lett. **95**, 107005 (2005).
[10] D. Gustafsson, D. Golubev, M. Fogelström, T. Claeson, S. Kubatkin, T. Bauch, and F. Lombardi, Nat. Nanotechnol. **8**, 25 (2013).
[11] R. Wölbing, T. Schwarz, J. Nagel, M. Kemmler, D. Koelle, and R. Kleiner, arXiv:1301.1189.
[12] J. Nagel, K. B. Konovalenko, M. Kemmler, M. Turad, R. Werner, E. Kleisz, S. Menzel, R. Klingeler, B. Büchner, R. Kleiner, and D. Koelle, Supercond. Sci. Technol. **24**, 015015 (2011).
[13] J. M. Martinis and R. L. Kautz, Phys. Rev. Lett. **63**, 1507 (1989); R. L. Kautz and J. M. Martinis, Phys. Rev. B **42**, 9903 (1990).
[14] J. M. Kivioja, T. E. Nieminen, J. Claudon, O. Buisson, F. W. J. Hekking, and J. P. Pekola, Phys. Rev. Lett. **94**, 247002 (2005); J. Mannik, S. Li, W. Qiu, W. Chen, V. Patel, S. Han, and J. E. Lukens, Phys. Rev. B **71**, 220509 (2005); V. M. Krasnov, T. Bauch, S. Intiso, E. Hurfeld, T. Akazaki, H. Takayanagi, and P. Delsing, Phys. Rev. Lett. **95**, 157002 (2005); J. C. Fenton and P. A. Warburton, Phys. Rev. B **78**, 054526 (2008); L. Longobardi, D. Massarotti, G. Rotoli, D. Stornaiuolo, G. P. Papari, A. Kawakami, G. P. Pepe, A. Barone, and F. Tafuri, *ibid.* **84**, 184504 (2011); Y. Kubo, A. O. Sboychakov, F. Nori, Y. Takahide, S. Ueda, I. Tanaka, A. T. M. N. Islam, and Y. Takano, *ibid.* **86**, 144532 (2012).
[15] H. F. Yu, X. B. Zhu, Z. H. Peng, Y. Tian, D. J. Cui, G. H. Chen, D. N. Zheng, X. N. Jing, L. Lu, S. P. Zhao, and S. Han, Phys. Rev. Lett. **107**, 067004 (2011).
[16] L. Longobardi, D. Massarotti, D. Stornaiuolo, L. Galletti, G. Rotoli, F. Lombardi, and F. Tafuri, Phys. Rev. Lett. **109**, 050601 (2012); D. Massarotti, L. Longobardi, L. Galletti, D. Stornaiuolo, G. Rotoli, and F. Tafuri, Low Temperature Physics **39**, 294 (2013).
[17] M. Iansiti, A. T. Johnson, W. F. Smith, H. Rogalla, C. J. Lobb, and M. Tinkham, Phys. Rev. Lett. **59**, 489 (1987); M. Iansiti, M. Tinkham, A. T. Johnson, W. F. Smith, and C. J. Lobb, Phys. Rev. B **39**, 6465 (1989).
[18] M. Tinkham, *Introduction to Superconductivity* (McGraw-Hill, New York, 1996).
[19] A. Y. Tzalenchuk, T. Lindstrom, S. A. Charlebois, E. A. Stepantsov, Z. Ivanov, and A. M. Zagoskin, Phys. Rev. B **68**, 100501 (2003); E. Il'ichev, M. Grajcar, R. Hlubina, R. P. J. IJsselsteijn, H. E. Hoenig, H. G. Meyer, A. Golubov, M. H. S. Amin, A. M. Zagoskin, A. N. Omelyanchouk, and M. Y. Kupriyanov, Phys. Rev. Lett. **86**, 5369 (2001); F. Herbstritt, T. Kemen, L. Alff, A. Marx, and R. Gross, Appl. Phys. Lett. **78**, 955 (2001); P. Larsson, B. Nilsson, and Z. G. Ivanov, J. Vac. Sci. Technol. B **18**, 25 (2000).
[20] D. Stornaiuolo, G. Papari, N. Cennamo, F. Carillo, L. Longobardi, D. Massarotti, A. Barone, and F. Tafuri, Superconductor Sci. Technol. **24**, 045008 (2011).
[21] D. Stornaiuolo, G. Rotoli, K. Cedergren, D. Born, T. Bauch, F. Lombardi, and F. Tafuri, J. Appl. Phys. **107**, 113901 (2010).
[22] F. Lombardi, F. Tafuri, F. Ricci, F. Miletto Granozio, A. Barone, G. Testa, E. Sarnelli, J. R. Kirtley, and C. C. Tsuei, Phys. Rev. Lett. **89**, 207001 (2002).

[23]F. M. Granozio, U. S. diUccio, F. Lombardi, F. Ricci, F. Bevilacqua, G. Ausanio, F. Carillo, and F. Tafuri, Phys. Rev. B **67**, 184506 (2003).

[24]F. Carillo, G. Papari, D. Stornaiuolo, D. Born, D. Montemurro, P. Pingue, F. Beltram, and F. Tafuri, Phys. Rev. B **81**, 054505 (2010); G. Papari, F. Carillo, D. Stornaiuolo, L. Longobardi, F. Beltram, and F. Tafuri, Supercond. Sci. Technol. **25**, 035011 (2012).

[25]F. Tafuri, F. Miletto Granozio, F. Carillo, A. Di Chiara, K. Verbist, and G. Van Tendeloo, Phys. Rev. B **59**, 11523 (1999).

[26]F. P. Milliken, J. R. Rozen, G. A. Keefe, and R. H. Koch, Rev. Sci. Instrum. **78**, 024701 (2007); L. Longobardi, D. A. Bennett, V. Patel, W. Chen, and J. E. Lukens, *ibid.* **84**, 014706 (2013).

[27]A. Barone and G. Paternò, *Physics and Applications of Josephson Effect* (Wiley, New York, 1982).

[28]P. A. Rosenthal, M. R. Beasley, K. Char, M. S. Colclough, and G. Zaharchuk, Appl. Phys. Lett. **59**, 26 (1991).

[29]The submicron junctions studied in this work have lower J_c when compared with the ones studied in Ref. 21. This difference is likely due to the different fabrication processes.

[30]T. Sakudo and H. Unoki, Phys. Rev. Lett. **26**, 851 (1971).

[31]G. Rotoli, T. Bauch, T. Lindstrom, D. Stornaiuolo, F. Tafuri, and F. Lombardi, Phys. Rev. B **75**, 144501 (2007).

[32]S. C. Tidrow, A. Tauber, W. D. Wilber, R. T. Lareau, C. D. Brandle, G. W. Berkstresser, A. J. Ven Graitis, D. M. Potrepka, J. I. Budnick, and J. Z. Wu, IEEE Trans. Appl. Supercond. **7**, 1766 (1997).

[33]R. H. Ono, M. W. Cromar, R. L. Kautz, R. J. Soulen, J. H. Colwell, and W. E. Fogle, IEEE Trans. Magn. **23**, 1670 (1987).

[34]M. H. Devoret, J. M. Martinis, and J. Clarke, Phys. Rev. Lett. **55**, 1908 (1985).

[35]A. J. Berkley, H. Xu, M. A. Gubrud, R. C. Ramos, J. R. Anderson, C. J. Lobb, and F. C. Wellstood, Phys. Rev. B **68**, 060502 (2003); J. Hassel, L. Grönberg, and P. Helistö, New J. Phys. **9**, 157 (2007); J. Delahaye, J. Hassel, R. Lindell, M. Sillanpää, M. Paalanen, H. Seppä, and P. Hakonen, Science **299**, 1045 (2003).

[36]The K-M model was just set to study phase diffusion as the natural simplest extension of the single-Q model. This cannot be achieved with a "shell" circuit approach, for example, the one reported in Ref. 31, which was implemented to model high-frequency response of YBCO junctions realized on STO substrates.

[37]See, http://wwwasdoc.web.cern.ch/wwwasdoc/shortwrupsdir/v115/top.html.

[38]D. Vion, M. Gotz, P. Joyez, D. Esteve, and M. H. Devoret, Phys. Rev. Lett. **77**, 3435 (1996).

[39]In Ref. 7 the Q of off-axis biepitaxial junctions was found to be 3.7 ± 1.1. This higher value is likely due to the fact that the junctions were realized on a STO substrate.

[40]The fact that in this last case we need to use a Q_0 fitting parameter of 12, which is larger than the value of 5 used for junction 1W, suggests an increase in effective resistance for device 6W, prevailing on the reduction of I_c. Iansiti *et al.* (Ref. 17) pointed out that, when charging effects become more relevant, the I-V characteristic becomes more resistive in the low-voltage regime.

[41]Quantum phase diffusion arises when E_c is comparable to E_J. This regime can be obtained by reducing either the I_c value or the capacitance of the junction. In our case, devices 1W and 6W are defined on the same chip, and the capacitance can reasonably assumed to be constant.

[42]A. O. Caldeira and A. J. Leggett, Phys. Rev. Lett. **46**, 211 (1981).

[43]A more quantitative analysis of the quantum phase diffusion regime for this device could be performed using SCD histograms. However, due to the low values of the critical currents, such measurements are extremely difficult to perform. As a matter of fact we are not aware of SCD measurements in this range of critical currents, even for LTS JJs.

[44]H. Grabert and U. Weiss, Phys. Rev. Lett. **53**, 1787 (1984).